



Cite this: DOI: 10.1039/c8nj06389c

3D hybrid perovskite solid solutions: a facile approach for deposition of nanoparticles and thin films *via* B-site substitution†

Muhammad Aamir,^a Rana Farhat Mehmood,^b Arshad Farooq Butt,^a Malik Dilshad Khan,^c Mohammad Azad Malik,^d Neerish Revaprasadu,^e Jean-Michel Nunzi,^e Muhammad Sher^f and Javeed Akhtar^{*a}

Mixed metal halide perovskites are gaining paramount interest due to efficient band gap tunability and improved optical properties compared to their single metal halide perovskites. It is thus valuable to investigate compositional changes in lead halide perovskites to explore energy changes. Herein, we report the synthesis of a lead to lead free hybrid perovskite solid solution ($\text{CH}_3\text{NH}_3\text{Pb}_{1-x}\text{Cu}_x\text{Br}_3$) as nanoparticles and films. The increasing concentration of Cu^{2+} ions in the site of the Pb^{2+} ion in the perovskite shifted the diffraction peaks to a larger angle. Uniform spherically shaped nanoparticles were synthesized by a wet chemical method, the higher Cu^{2+} concentration leads to agglomeration, producing sheet like morphologies. However, the deposition of thin films of $\text{CH}_3\text{NH}_3\text{Pb}_{1-x}\text{Cu}_x\text{Br}_3$ perovskite solid solution shows that well defined morphologies begin to appear with increasing concentrations of Cu^{2+} in the perovskite structure. The as-prepared bulk lead free $\text{CH}_3\text{NH}_3\text{CuBr}_3$ perovskite shows a band gap of 1.65 eV. A blue shift in photoluminescence (PL) was observed with copper enriched hybrid perovskites.

Received 25th December 2018,
Accepted 11th March 2019

DOI: 10.1039/c8nj06389c

rsc.li/njc

Introduction

The recent, robust development of perovskite materials has revolutionized the photovoltaics research field with the highest certified solar light conversion efficiency reported to be over 20%.^{1–4} Metal halide perovskites exhibit ideal properties for applications including photovoltaics,^{5,6} sensing,^{7–9} photocatalysis,¹⁰ piezoelectrics^{11,12} and lasing¹³ due to a tunable band gap,^{14,15} low exciton binding energy,^{16,17} long carrier diffusion lengths^{18,19} and broad band emission.^{20,21} Despite the record efficiency, one major concern with this material is the toxicity of lead. Therefore, a key challenge is to replace lead with less toxic metals, however, no compatible success has been reported so far.

Although, Pb has been replaced with its group members, Sn and Ge, the stability of the 2+ oxidation state decreases while moving up this group, which limits the use of these metals in the synthesis of stable metal halide perovskites. In particular, Sn has been widely studied as an alternative to Pb, but, it undergoes oxidation from Sn^{2+} to Sn^{4+} in which Sn^{4+} act as a p-type dopant by a self-doping process.^{22–24} The partial incorporation of Sn in the $\text{CH}_3\text{NH}_3\text{PbI}_3$ perovskite tunes the optical properties.²³ Recently, Zhang *et al.*²⁵ have reported the gradual substitution of Sb^{3+} in the Pb^{2+} site of $\text{CH}_3\text{NH}_3\text{PbI}_3$ perovskites to tailor the optoelectronic properties, and tuned the band gap from 1.55 eV to 2.06 eV. However, the complete interconversion of $\text{CH}_3\text{NH}_3\text{PbI}_3$ to the layered $\text{CH}_3\text{NH}_3\text{Sb}_{0.66}\text{I}_3$ perovskite leads to reduced photovoltaic efficiency. Only 1% Sb doping in $\text{CH}_3\text{NH}_3\text{PbI}_3$ was found to improve the V_{oc} , FF and I_{sc} of the solar cell.²⁵ These shortcomings drew the attention of the scientific community to exploring other substitutes for Pb. Transition metals, particularly attractive metals, such as, Fe^{2+} , Cu^{2+} *etc.* can be used to investigate potential alternatives to lead-based perovskites. Taking this into consideration there is an urge to develop alternative transition metal based perovskites due to their chemical stability, reduced toxicity and abundance.

Herein, we have attempted for the first time, the synthesis, characterization and fabrication of nanoparticles and bulk perovskite solid solutions obtained by the incorporation of

^a Materials laboratory, Department of Chemistry, Mirpur University of Science & Technology (MUST), Mirpur-10250 (AJK), Pakistan.

E-mail: javeed.chem@must.edu.pk

^b Department of Chemistry, University of Education Lahore, Dera Ghazi Khan Campus, Kangan Road, DG Khan, Pakistan

^c Department of Chemistry, University of Zululand, Private Bag X1001, Kwadlangezwa, 3886, South Africa

^d School of Materials, The University of Manchester, Oxford Road, M13 9PL, UK

^e Department of Chemistry, Queen's University, Kingston, ON K7L 3N6, Canada

^f Department of Chemistry, Allama Iqbal Open University, Islamabad, Pakistan

† Electronic supplementary information (ESI) available. See DOI: 10.1039/c8nj06389c

Cu^{2+} in the site of Pb^{2+} ions to produce a $\text{CH}_3\text{NH}_3\text{Pb}_{1-x}\text{Cu}_x\text{Br}_3$ series. The aim is to study the sequential effects on the optical, morphological and structural properties which may provide a basis to optimize the conditions for the photovoltaic applications of lead free $\text{CH}_3\text{NH}_3\text{CuBr}_3$.

Experimental

Materials

Lead bromide, copper bromide, methylamine, hydrogen bromide, diethyl ether, *N,N* dimethylformamide, acetone, octylamine and *n*-hexane were purchased from Sigma Aldrich and used without further purification.

Characterization

p-XRD measurements were performed using a Bruker aXS D8 advanced diffractometer with $\text{Cu-K}\alpha$ radiation ($\lambda = 1.5406 \text{ \AA}$) operated at 40 kV and 40 mA. Scanning electron microscopy (SEM) was carried out using a Philips XL30 FEG SEM. Energy-dispersive analysis of X-rays (EDAX) spectroscopy was performed using a DX4 detector. All samples were carbon coated using the Edwards coating system E306A prior to SEM analysis. A PerkinElmer Lambda 20 UV-Vis spectrophotometer was used to carry out optical measurements in the 200–1100 nm wavelength range at room temperature. Samples were placed in quartz cuvettes (1 cm path length) and absorbance was recorded. Photoluminescence (PL) spectra were recorded on a PerkinElmer LS 55 luminescence spectrometer with xenon lamp over the range of 200–800 nm. The XPS spectra were measured on a Microlab 310-F spectrometer equipped with an XR-4 twin anode (Al/Mg). The manufacturer of this system is VG Scientific. The samples were mounted on a stub-type stainless steel holder using double-sided adhesive Cu tape and kept under high vacuum (10^{-8} mbar) overnight inside the preparation chamber before they were transferred into the analysis chamber (10^{-9} mbar) of the spectrometer. The XPS data were collected using Mg $\text{K}\alpha$ radiation at 1253.6 eV (280 W, 14 kV) and a spherical sector analyzer (SSA) operating in CAE (constant analyzer energy) mode. Survey spectra were recorded from –5 to 1000 eV at a pass energy of 40 eV (number of scans: 5) using an energy step size of 2 eV. High resolution spectra were measured for C 1s, N 1s, Br 3d, and Cu 2p in the appropriate regions at a pass energy of 20 eV and an energy step size of 0.05 eV. The analyzed area on the specimens was about $5 \times 2 \text{ mm}^2$.

Synthesis of methylammonium bromide ($\text{CH}_3\text{NH}_3\text{Br}$)

The synthesis of methylammonium bromide was carried out by reacting 15.0 mL of methylamine (40% solution in water) and 20.0 mL of hydrogen bromide (48% solution in water) in a round bottom flask. The reaction was stirred for two hours in an ice bath. The solvent was evaporated using a rotary evaporator and the product recrystallized with ethanol. The obtained product was washed twice with diethyl ether and then dried at 60 °C for 24 hours.

Synthesis of $\text{CH}_3\text{NH}_3\text{Pb}_{1-x}\text{Cu}_x\text{Br}_3$ nanoparticles

The methylammonium lead bromide nanoparticles were synthesized by dissolving 0.0367 g (0.1 mmol) of PbBr_2 and 0.0112 g (0.1 mmol) of $\text{CH}_3\text{NH}_3\text{Br}$ in 2.0 mL of octadecene with 1.0 mL of oleic acid and 0.0126 g of octylammonium bromide at room temperature with stirring. The copper substitution was then performed by a successive increase of copper bromide by 20%, while decreasing the amount of lead bromide by the same amount in the reaction mixture, keeping the $\text{CH}_3\text{NH}_3\text{Br}/\text{MBr}_2$ ratio constant at 1 : 1. After 2.0 minutes of reaction time, 10.0 mL of acetone was added into the reaction mixture with stirring to obtain the precipitates. The obtained precipitates were then centrifuged at 10 000 rpm for 10 minutes and then dispersed in hexane, followed by washing with acetone and centrifugation to get a colloidal suspension in toluene for further characterization.

Deposition of $\text{CH}_3\text{NH}_3\text{Pb}_{1-x}\text{Cu}_x\text{Br}_3$ thin films

To deposit perovskite bulk derivatives, a glass substrate was cleaned by sonication for 15 minutes in a detergent, isopropanol and acetone, respectively. 0.1 mM of perovskite was dissolved in 1.0 mL of DMF with stirring for 1 hour. The copper substitution in $\text{CH}_3\text{NH}_3\text{PbBr}_3$ was carried out by adding a calculated amount of copper bromide by substituting the lead precursor in the reaction mixture. The as-prepared $\text{CH}_3\text{NH}_3\text{Pb}_{1-x}\text{Cu}_x\text{Br}_3$ perovskite derivatives were then spin coated at 3000 rpm for 30 seconds and then annealed at 100 °C for 10 minutes.

Results and discussion

The synthesis of nanoparticles and deposition of thin films of bulk $\text{CH}_3\text{NH}_3\text{Pb}_{1-x}\text{Cu}_x\text{Br}_3$ perovskites were carried out with an approach to develop lead free hybrid perovskites and to study their phase, shape and morphological effects. In the reaction to substitute copper in the lead based hybrid perovskite nanoparticles, copper bromide was added with lead bromide to control the concentration ratio of metal cations.

The $\text{CH}_3\text{NH}_3\text{PbBr}_3$ nanoparticles were yellow in color, but with the Pb-site substitution with copper, the color of the as-prepared nanoparticles started to change to green and then to violet on complete conversion to $\text{CH}_3\text{NH}_3\text{CuBr}_3$. In this study, the collection of $\text{CH}_3\text{NH}_3\text{CuBr}_3$ nanoparticles was unsuccessful. Repeated attempts to precipitate the nanoparticles by using different polar or non-polar solvents such as acetone, *n*-hexane, methanol, chloroform, cyclohexane and mixtures of solvents, were unsuccessful.

Powder-XRD was performed to determine the effect of copper substitution on the crystalline structure of lead based hybrid perovskites. The as-prepared $\text{CH}_3\text{NH}_3\text{PbBr}_3$ nanoparticles showed diffraction peaks at $2\theta = 15.14^\circ$ (001), 21.39° (011), 30.35° (002), 34.01° (021), 37.35° (211), 43.31° (022), 46.08° (221) and 48.78° (031) representing the cubic phase of the perovskite structure as shown in Fig. 1(a). All observed peaks belong to the cubic phase of $\text{CH}_3\text{NH}_3\text{PbBr}_3$ with no extra phases and are in agreement with the literature.^{14,26} However, for the successive substitution of copper

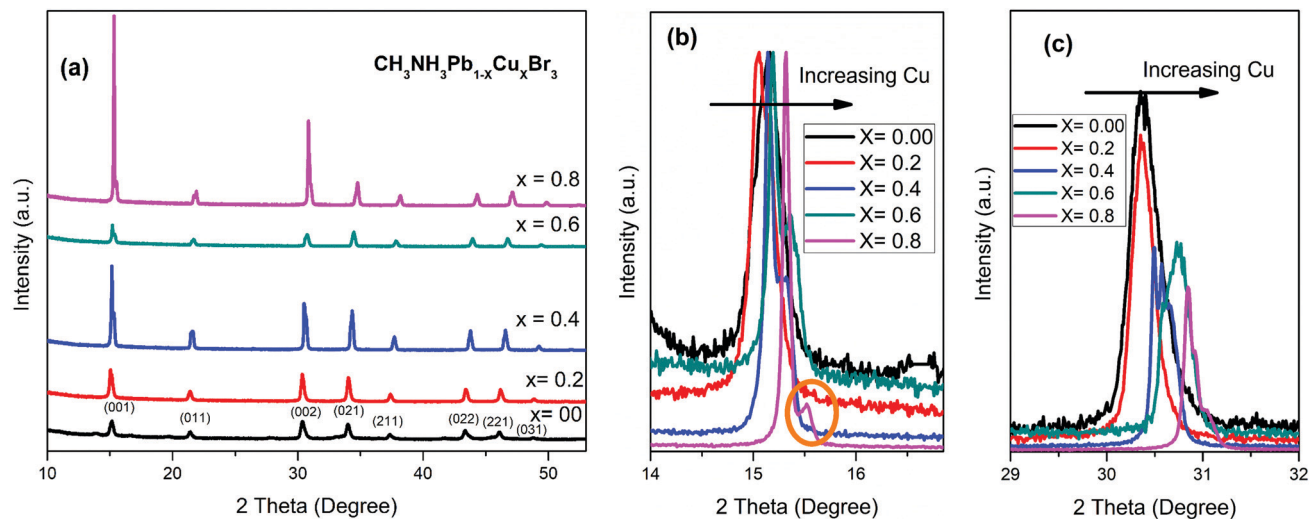


Fig. 1 XRD spectra of the $\text{CH}_3\text{NH}_3\text{Pb}_{1-x}\text{Cu}_x\text{Br}_3$ nanoparticles by substituting Pb with Cu. (a) Complete spectra presenting the complete range of interest. (b and c) Magnification of the peaks centered at around 21.3° (b) and 30.3° (c).

in the lead based perovskite, the diffraction peaks started shifting gradually from a lower angle to a higher angle. The concentrations of copper and the respective shifts in diffraction peaks are presented in Table 1. The shifting of the peaks is due to the smaller ionic size of the copper ion (ionic radii = 73 pm)²⁷ compared to that of the lead ion (ionic radii = 119 pm).²⁷ Fig. 1(b) shows the p-XRD spectra of nanoparticles with magnification of the peak centered near $2\theta = 15^\circ$ and Fig. 1(c) shows the magnification of the peak around $2\theta = 30^\circ$. These peaks belong to the (001) and (002) planes of the cubic $\text{CH}_3\text{NH}_3\text{PbBr}_3$ perovskite phase. The prominent shifts in the aforementioned diffraction peaks were observed when the Pb:Cu molar ratio was 0.6:0.4 ($\text{CH}_3\text{NH}_3\text{Pb}_{0.6}\text{Cu}_{0.4}\text{Br}_3$) as presented in Fig. 1(b and c). However, the shoulder peaks at $2\theta = 15.31^\circ$ and 21.58° may be due to the phase segregation process.

Fig. S1(a–f) (ESI[†]) shows the TEM images of the as-prepared nanoparticles of $\text{CH}_3\text{NH}_3\text{Pb}_{1-x}\text{Cu}_x\text{Br}_3$ hybrid perovskite derivatives. The nanoparticles synthesized at room temperature have uniform spherical morphology and are monodispersed with an average size of 12 ± 1 nm. The increase in molar ratio of Cu^{2+} and decrease in Pb^{2+} (Pb:Cu = 0.8:0.2, 0.6:0.4, 0.4:0.6, and 0.2:0.8) keeps the overall shape of particles as spherical (Fig. S1a–e, ESI[†]). However, larger particles appeared due to aggregation in $\text{CH}_3\text{NH}_3\text{Pb}_{0.6}\text{Cu}_{0.4}\text{Br}_3$, $\text{CH}_3\text{NH}_3\text{Pb}_{0.4}\text{Cu}_{0.6}\text{Br}_3$, and $\text{CH}_3\text{NH}_3\text{Pb}_{0.2}\text{Cu}_{0.8}\text{Br}_3$ (Fig. S1(c–e), ESI[†]). The copper addition may increase the rate of nucleation and enhance the

growth of the nanoparticles, which results in larger particles. The complete conversion to $\text{CH}_3\text{NH}_3\text{CuBr}_3$ perovskite produced nanoparticles of more than 100 nm size with elongated shapes due to the merging of smaller particles (Fig. S1(f), ESI[†]). The inset in Fig. S1(f) (ESI[†]) shows that the $\text{CH}_3\text{NH}_3\text{CuBr}_3$ perovskite undergoes anisotropic growth to form sheet like morphologies. These results suggest that the copper may facilitate faster nucleation and promote large structure formation.

The optical properties of the as-synthesized nanoparticles of $\text{CH}_3\text{NH}_3\text{Pb}_{1-x}\text{Cu}_x\text{Br}_3$ perovskite derivatives were examined in detail with successive increases in copper concentration. During the conversion of $\text{CH}_3\text{NH}_3\text{PbBr}_3$ to lead free $\text{CH}_3\text{NH}_3\text{CuBr}_3$ perovskites, a slight change in the absorption spectra was observed as shown in Fig. S2(a) (ESI[†]). Whereas, the main change was observed in photoluminescence (PL) as shown in Fig. S2(b) (ESI[†]). The $\text{CH}_3\text{NH}_3\text{PbBr}_3$ nanoparticles showed a single emission peak at 508 nm. The emission intensity of this peak was decreased in the $\text{CH}_3\text{NH}_3\text{Pb}_{0.8}\text{Cu}_{0.2}\text{Br}_3$ perovskite with the appearance of a new peak at 506 nm, which may be due to trap states generated by the copper ion. The gradual increase of the copper ratio results in a decrease of emission intensity peaked at 508 nm and a slight blue shift in the peak at 508 nm. In addition, a new peak at 392 nm appeared for compound $\text{CH}_3\text{NH}_3\text{Pb}_{0.6}\text{Cu}_{0.4}\text{Br}_3$ along with a blue shifted low intensity peak at 502 nm. In compound $\text{CH}_3\text{NH}_3\text{Pb}_{0.4}\text{Cu}_{0.6}\text{Br}_3$ three peaks appeared, which were labelled at 492 nm, 444 nm and 392 nm. These peaks were of low intensity suggesting that copper

Table 1 p-XRD diffraction peaks of $\text{CH}_3\text{NH}_3\text{Pb}_{1-x}\text{Cu}_x\text{Br}_3$ perovskite derivatives

Perovskite	Copper [x]	pXRD diffraction peaks									
		(001)	—	(011)	—	(002)	(021)	(211)	(022)	(221)	(031)
$\text{CH}_3\text{NH}_3\text{PbBr}_3$	0	15.14°	—	21.39°	—	30.35°	34.01°	37.35°	43.31°	46.08°	48.78°
$\text{CH}_3\text{NH}_3\text{Pb}_{0.8}\text{Cu}_{0.2}\text{Br}_3$	0.2	15.05°	—	21.40°	—	30.35°	34.04°	37.40°	43.42°	46.18°	48.87°
$\text{CH}_3\text{NH}_3\text{Pb}_{0.6}\text{Cu}_{0.4}\text{Br}_3$	0.4	15.14°	15.31°	21.52°	21.58°	30.49°	34.35°	37.70°	43.77°	46.57°	49.26°
$\text{CH}_3\text{NH}_3\text{Pb}_{0.4}\text{Cu}_{0.6}\text{Br}_3$	0.6	15.19°	15.35°	21.54°	21.72°	30.72°	34.48°	37.83°	43.96°	46.77°	49.45°
$\text{CH}_3\text{NH}_3\text{Pb}_{0.2}\text{Cu}_{0.8}\text{Br}_3$	0.8	15.31°	15.51°	21.68°	21.89°	30.84°	34.77°	38.19°	44.31°	47.14°	49.86°

halide rich perovskites could be weak emitters. The PL emission spectrum of $\text{CH}_3\text{NH}_3\text{Pb}_{0.2}\text{Cu}_{0.8}\text{Br}_3$ showed multiple low intensity peaks located at 485 nm, 436 nm, 425 nm and 392 nm. However, for the $\text{CH}_3\text{NH}_3\text{CuBr}_3$ perovskite, the peak at 485 nm disappeared and there were slight intense peaks at 425 nm and 392 nm. The drop in PL intensity with increasing copper may be due to the transformation of charge carries from lead based to copper based perovskite parts.

To further understand the structural and morphological evolution in B-site substituted hybrid perovskites using copper, we deposited bulk $\text{CH}_3\text{NH}_3\text{Pb}_{1-x}\text{Cu}_x\text{Br}_3$ perovskite thin films using a single step spin coating method. The solution concentration was kept deliberately low, to understand the effect of copper substitution on the morphology and crystallization in the as-prepared hybrid perovskite derivatives. Crystal structure analysis was performed using p-XRD analysis as shown in Fig. 2(a). The diffraction peaks at $2\theta = 14.46^\circ$, 20.70° , 29.69° , 33.36° , 42.77° and 45.49° were assigned to the (110), (200), (220), (310), (224) and (314) planes of the tetragonal perovskite phase of compound $\text{CH}_3\text{NH}_3\text{PbBr}_3$. The shifting of diffraction peaks to higher angles was observed with the increase of copper as shown in Fig. 2(b) and (c). Prominent changes in the diffraction peaks appeared after a Pb:Cu molar ratio of 0.6:0.4. Two new peaks appeared at $2\theta = 27.29^\circ$ and 36.85° in the diffraction pattern of $\text{CH}_3\text{NH}_3\text{Pb}_{0.6}\text{Cu}_{0.4}\text{Br}_3$, which were further intensified when moving towards the $\text{CH}_3\text{NH}_3\text{CuBr}_3$ end of the series. However, phase segregation was absent in bulk thin films.

The p-XRD pattern of $\text{CH}_3\text{NH}_3\text{CuBr}_3$ shows the complete absence of peaks at $2\theta = 29.69^\circ$, 33.36° , 42.77° , 14.46° and 20.70° which were observed in the lead based perovskite.

Table 2 shows the change in diffraction peaks of $\text{CH}_3\text{NH}_3\text{Pb}_{1-x}\text{Cu}_x\text{Br}_3$ perovskites with the addition of copper ions.

XPS measurements were performed to determine the elemental composition and oxidation state of Cu in the $\text{CH}_3\text{NH}_3\text{CuBr}_3$ perovskite bulk films. The XPS spectrum for $\text{CH}_3\text{NH}_3\text{CuBr}_3$ shows peaks located at binding energies of 532 eV, 402 eV and 286 eV belonging to photoelectronic peaks of O 1s, N 1s and C 1s respectively. Whereas, peaks around 930 eV and 69 eV corresponded to the Cu and Br, respectively.

Fig. 3(a) shows the XPS spectra of C 1s binding energy for adventitious carbon (aliphatic).²⁸ After linear background subtraction, the core level spectra were fitted using Gaussian line shapes. The C 1s spectrum of $\text{CH}_3\text{NH}_3\text{CuBr}_3$ showed three peaks located at 284.93 eV, 285.78 eV and 286.64 eV. The peak at 284.93 eV is known as adventitious carbon or absorbed surface hydrocarbon from the atmosphere.²⁸ While, the peak at 285.78 eV belongs to the methyl carbon of $\text{CH}_3\text{NH}_3\text{CuBr}_3$ or possibly the methyl groups singly bonded to the hydroxyl group.²⁹ Another peak appeared at 286.64 eV corresponding to the carbon double bonded to oxygen, which is also due to surface contamination.

Fig. 3(b) shows the XPS spectrum of O 1s binding energy for the $\text{CH}_3\text{NH}_3\text{CuBr}_3$ perovskite film. The O 1s spectrum shows three peaks located at 531.08 eV, 532.04 eV, and 532.98 eV. Among these peaks, the two peaks found at 531.08 eV and 532.98 eV correspond to C=O, and O=C-O respectively.³⁰ These peaks typically appear in the air exposed samples and the carbons are known as adventitious carbons containing various hydrocarbon species with both saturated and unsaturated carbon oxygen functionalities. The peak at 531.08 eV appeared

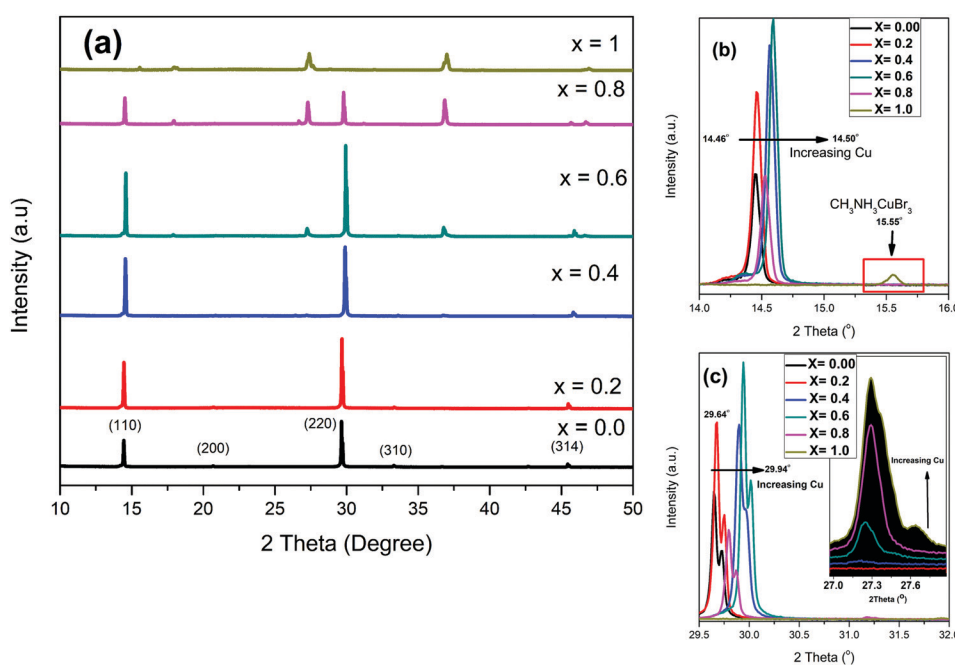


Fig. 2 p-XRD pattern of the $\text{CH}_3\text{NH}_3\text{Pb}_{1-x}\text{Cu}_x\text{Br}_3$ thin films by substituting Pb with Cu. (a) Complete pattern of as-deposited perovskite derivatives. (b) and (c) Magnifications of the peaks centered at 14.5° (b) and near 25.6° (c), whereas, inset of (c) is the magnification of peak at 27.3° .

Table 2 pXRD peak position in the bulk $\text{CH}_3\text{NH}_3\text{Pb}_{1-x}\text{Cu}_x\text{Br}_3$ perovskite derivative thin films

Perovskite	Copper [x]	pXRD diffraction peaks								
		(110)	(200)	(220)	(310)	(224)	(314)			
$\text{CH}_3\text{NH}_3\text{PbBr}_3$	0	14.46°	20.70°	29.69°	33.36°	42.77°	45.49°			
$\text{CH}_3\text{NH}_3\text{Pb}_{0.8}\text{Cu}_{0.2}\text{Br}_3$	0.2	14.48°	20.70°	29.72°	33.37°	—	45.54°			
$\text{CH}_3\text{NH}_3\text{Pb}_{0.6}\text{Cu}_{0.4}\text{Br}_3$	0.4	14.49°	17.93°	27.29°	29.73°	33.41°	36.85°	45.55°		
$\text{CH}_3\text{NH}_3\text{Pb}_{0.4}\text{Cu}_{0.6}\text{Br}_3$	0.6	14.50°	17.93°	27.29°	29.76°	—	36.85°	45.60°		
$\text{CH}_3\text{NH}_3\text{Pb}_{0.2}\text{Cu}_{0.8}\text{Br}_3$	0.8	14.50°	17.93°	27.29°	29.76°	—	36.85°	34.77°		
$\text{CH}_3\text{NH}_3\text{CuBr}_3$	0	—	17.93°	27.29°	—	—	36.85°	—		

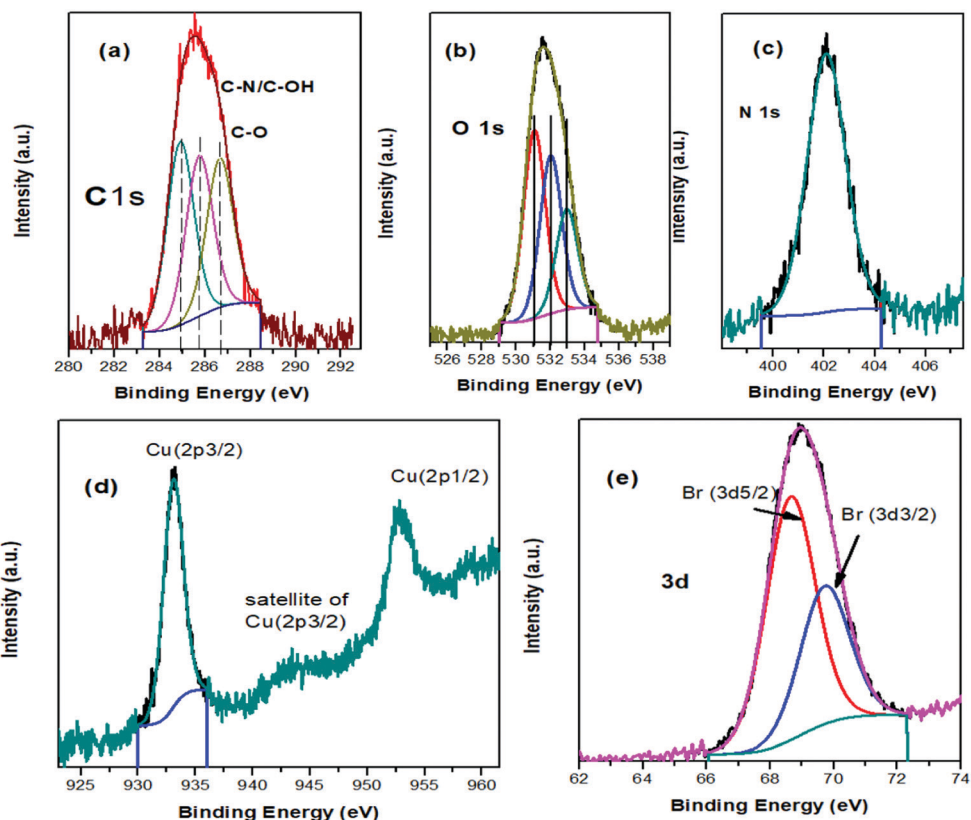


Fig. 3 XPS analysis representing the electronic binding energies of (a) carbon, (b) oxygen, (c) nitrogen, (d) copper and (e) bromine in $\text{CH}_3\text{NH}_3\text{CuBr}_3$ perovskite.

mainly due to the weakly absorbed OH^- and O^{2-} ions, and can also be related to the Cu(II)-O/Cu(OH)_2 like states.³¹ The formation of $\text{Cu(II)-O/Cu(II)-OH}$ like states indicates surface oxidation, where dissociated oxygen species or chemisorbed oxygen moieties can diffuse into the $\text{CH}_3\text{NH}_3\text{CuBr}_3$ structure which results in distortion and degradation of the perovskite structure. Consequently, the decrease in the concentration of bromide ions at the surface of the $\text{CH}_3\text{NH}_3\text{CuBr}_3$ film was observed. The atomic % of the $\text{CH}_3\text{NH}_3\text{CuBr}_3$ calculated by XPS shows around 25% of oxygen moieties, which suggest that the as-deposited compound has easy diffusion of oxygen into the $\text{CH}_3\text{NH}_3\text{CuBr}_3$ thin film. The XPS spectrum of N 1s shows a characterization peak located at a binding energy of 402 eV (Fig. 3(c)).

Fig. 3(d) shows the XPS spectra of Cu in $\text{CH}_3\text{NH}_3\text{CuBr}_3$ thin films. The Cu ($2p_{3/2}$) and Cu ($2p_{1/2}$) peaks positioned at

933.15 eV and 952.73 eV respectively indicate the presence of Cu^{2+} . Furthermore, the satellite peak of Cu ($2p_{3/2}$) at 943.39 eV confirms the 2+ oxidation state of the copper.³¹ The XPS spectrum of core level Br 3d exhibits two peaks located at 68.68 eV and 69.77 eV corresponding to $3d_{5/2}$ and $3d_{3/2}$, respectively (Fig. 3(e)).

The SEM images (Fig. S3(a–f) ESI[†]) of the as-deposited thin films show the significant change in morphology with the increase in copper in the hybrid perovskite. The observance of flake-like grains of $\text{CH}_3\text{NH}_3\text{PbBr}_3$ crystallites is shown in Fig. S3(a) (ESI[†]) and is well discussed in the literature.^{26,32} The $\text{CH}_3\text{NH}_3\text{PbBr}_3$ perovskite flake-like grains can cover the surface of the substrate to form uniform pinhole free thin films with a small modification in the deposition process. However, it was observed that more crystalline edges and crystal formation starts to appear as the Pb:Cu molar ratio reached to 0.8:0.2

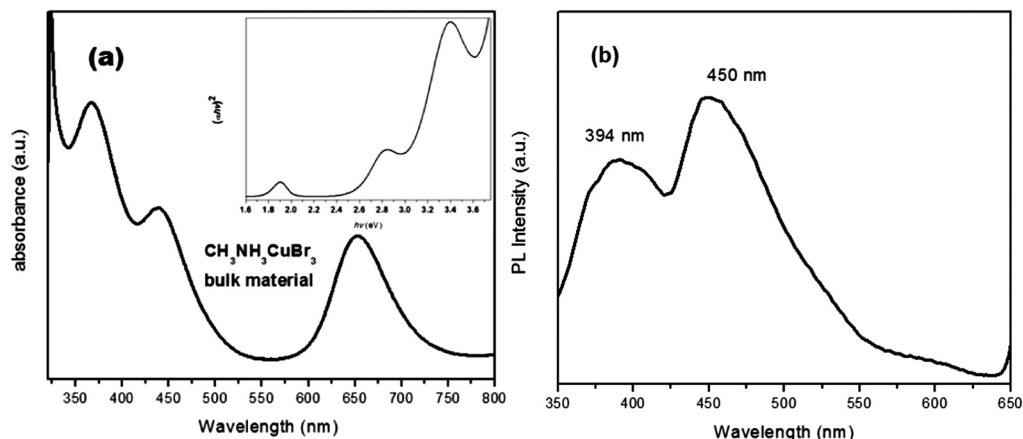


Fig. 4 (a) UV-Vis absorption, inset is the Tauc plot and (b) PL spectra of bulk $\text{CH}_3\text{NH}_3\text{CuBr}_3$ perovskite.

($\text{CH}_3\text{NH}_3\text{Pb}_{0.8}\text{Cu}_{0.2}\text{Br}_3$ perovskite) as shown in Fig. S3(b) (ESI[†]). The increase in copper concentration produces cubic shaped morphologies (Fig. S3(b–d)) (ESI[†]), however, when the molar ratio reaches 0.4:0.6, some star shaped crystallites also appeared as shown in Fig. S3(d) (ESI[†]).

A flower-like growth of particles was observed in the thin film of $\text{CH}_3\text{NH}_3\text{Pb}_{0.2}\text{Cu}_{0.8}\text{Br}_3$ (Fig. S3(e) (ESI[†])) with a Pb:Cu molar ratio of 0.2:0.8, suggesting that the copper ions affect the morphology more effectively than the lead ions. Finally, the lead free $\text{CH}_3\text{NH}_3\text{CuBr}_3$ perovskite thin film shows small crystalline rice-like structures which were well dispersed on the glass substrate. The formation of these structures suggests that the copper based hybrid perovskite forms a crystal, which may lead to exposed surfaces of the glass substrate and may result in thin films containing pinholes as shown in Fig. S3(f) (ESI[†]). This observation could provide a basis to optimize the deposition parameters to obtain films with complete surface coverage during the fabrication of a $\text{CH}_3\text{NH}_3\text{CuBr}_3$ solar cell.

The UV-Vis absorption spectrum of the $\text{CH}_3\text{NH}_3\text{CuBr}_3$ perovskite is shown in Fig. 4(a). The as-prepared compound $\text{CH}_3\text{NH}_3\text{CuBr}_3$ shows three distinct absorption peaks located at 653 nm, 438 nm and 367 nm. The appearance of three absorption peaks is probably due to the distortion of the CuBr_6^- anion and the Jahn–Teller effect in this perovskite. In the inset of Fig. 4(a), the Tauc plot shows that the band gaps of the as-synthesized $\text{CH}_3\text{NH}_3\text{CuBr}_3$ perovskite are about 1.65 eV, 2.53 eV and 2.93 eV. The 1.65 eV bandgap is close to the band gap of $\text{CH}_3\text{NH}_3\text{PbI}_3$ perovskite (1.55 eV).^{33,34} Fig. 4(b) shows the PL emission spectrum of $\text{CH}_3\text{NH}_3\text{CuBr}_3$ perovskites excited at 330 nm, and two emission peaks located at 394 nm and 450 nm were observed. The appearance of two emission peaks may also arise due to the Jahn–Teller effect.

Conclusions

In summary, we have incorporated divalent Cu in the site of Pb in a hybrid perovskite to synthesize a solid solutions of a range of $\text{CH}_3\text{NH}_3\text{Pb}_{1-x}\text{Cu}_x\text{Br}_3$ in the form of nanoparticles and thin

films. It was observed that the gradual increasing of Cu^{2+} leads to a shift in the diffraction peaks to longer theta values, both in the films and the nanoparticles. The uniform spherically shaped nanoparticles with sizes of 12 ± 1 nm were successfully synthesized using oleic acid as a capping agent. The increasing concentration of Cu^{2+} enlarges the size of the nanoparticles without affecting the shape. However, the films showed different morphologies with increasing Cu^{2+} concentration. The band gap of the $\text{CH}_3\text{NH}_3\text{CuBr}_3$ perovskite was calculated to be 1.65 eV which found to be closer to $\text{CH}_3\text{NH}_3\text{PbI}_3$ perovskite (1.55 eV). In addition, the increasing amount of Cu^{2+} also shifts the PL to shorter wavelengths (blue shift). These results can provide a basis to establish lead free $\text{CH}_3\text{NH}_3\text{CuBr}_3$ perovskites as alternative less toxic photovoltaic perovskite materials.

Conflicts of interest

There are no conflicts to declare.

Acknowledgements

M. Aamir thanks the Higher Education Commission (HEC) of Pakistan for funding under start-up research grant program (SRGP) (Grant # 2262). JA acknowledges the funding from the HEC, Pakistan under NRUP/R&D/2017-project #8227.

References

- 1 A. Kojima, K. Teshima, Y. Shirai and T. Miyasaka, *J. Am. Chem. Soc.*, 2009, **131**, 6050–6051.
- 2 N. J. Jeon, J. H. Noh, W. S. Yang, Y. C. Kim, S. Ryu, J. Seo and S. I. Seok, *Nature*, 2015, **517**, 476–480.
- 3 M. Saliba, T. Matsui, J.-Y. Seo, K. Domanski, J.-P. Correa-Baena, M. K. Nazeeruddin, S. M. Zakeeruddin, W. Tress, A. Abate and A. Hagfeldt, *Energy Environ. Sci.*, 2016, **9**, 1989–1997.

- 4 M. Aamir, T. Adhikari, M. Sher, M. D. Khan, J. Akhtar and J. M. Nunzi, *Chem. Rec.*, 2018, **18**, 230–238.
- 5 M. Aamir, T. Adhikari, M. Sher, N. Revaprasadu, W. Khalid, J. Akhtar and J.-M. Nunzi, *New J. Chem.*, 2018, **42**, 14104–14110.
- 6 M. B. Johnston and L. M. Herz, *Acc. Chem. Res.*, 2015, **49**, 146–154.
- 7 M. Aamir, M. Sher, M. A. Malik, J. Akhtar and N. Revaprasadu, *New J. Chem.*, 2016, **40**, 9719–9724.
- 8 M. Aamir, M. Sher, M. A. Malik, N. Revaprasadu and J. Akhtar, *Mater. Lett.*, 2016, **183**, 135–138.
- 9 M. Aamir, M. D. Khan, M. Sher, S. V. Bhosale, M. A. Malik, J. Akhtar and N. Revaprasadu, *Eur. J. Inorg. Chem.*, 2017, 3755–3760.
- 10 M. Aamir, Z. H. Shah, M. Sher, A. Iqbal, N. Revaprasadu, M. A. Malik and J. Akhtar, *Mater. Sci. Semicond. Process.*, 2017, **63**, 6–11.
- 11 Y.-M. You, W.-Q. Liao, D. Zhao, H.-Y. Ye, Y. Zhang, Q. Zhou, X. Niu, J. Wang, P.-F. Li and D.-W. Fu, *Science*, 2017, **357**, 306–309.
- 12 W.-Q. Liao, Y.-Y. Tang, P.-F. Li, Y.-M. You and R.-G. Xiong, *J. Am. Chem. Soc.*, 2017, **139**, 18071–18077.
- 13 S. Yakunin, L. Protesescu, F. Krieg, M. I. Bodnarchuk, G. Nedelcu, M. Humer, G. De Luca, M. Fiebig, W. Heiss and M. V. Kovalenko, *Nat. Commun.*, 2015, **6**, 8056.
- 14 T. Baikie, Y. Fang, J. M. Kadro, M. Schreyer, F. Wei, S. G. Mhaisalkar, M. Graetzel and T. J. White, *J. Mater. Chem. A*, 2013, **1**, 5628–5641.
- 15 G. E. Eperon, S. D. Stranks, C. Menelaou, M. B. Johnston, L. M. Herz and H. J. Snaith, *Energy Environ. Sci.*, 2014, **7**, 982–988.
- 16 C. S. Ponseca Jr, T. J. Savenije, M. Abdellah, K. Zheng, A. Yartsev, T. r. Pascher, T. Harlang, P. Chabera, T. Pullerits and A. Stepanov, *J. Am. Chem. Soc.*, 2014, **136**, 5189–5192.
- 17 A. Miyata, A. Mitioglu, P. Plochocka, O. Portugall, J. T.-W. Wang, S. D. Stranks, H. J. Snaith and R. J. Nicholas, *Nat. Phys.*, 2015, **11**, 582–587.
- 18 S. D. Stranks, G. E. Eperon, G. Grancini, C. Menelaou, M. J. Alcocer, T. Leijtens, L. M. Herz, A. Petrozza and H. J. Snaith, *Science*, 2013, **342**, 341–344.
- 19 G. Xing, N. Mathews, S. Sun, S. S. Lim, Y. M. Lam, M. Grätzel, S. Mhaisalkar and T. C. Sum, *Science*, 2013, **342**, 344–347.
- 20 M. Aamir, M. D. Khan, M. Sher, N. Revaprasadu, M. A. Malik and J. Akhtar, *New J. Chem.*, 2018, **42**, 17181–17184.
- 21 M. Aamir, M. D. Khan, M. Sher, M. A. Malik, J. Akhtar and N. Revaprasadu, *ChemistrySelect*, 2017, **2**, 5595–5599.
- 22 Q. Jiang, D. Rebolgar, J. Gong, E. L. Piacentino, C. Zheng and T. Xu, *Angew. Chem.*, 2015, **127**, 7727–7730.
- 23 Y. Ogomi, A. Morita, S. Tsukamoto, T. Saitho, N. Fujikawa, Q. Shen, T. Toyoda, K. Yoshino, S. S. Pandey and T. Ma, *J. Phys. Chem. Lett.*, 2014, **5**, 1004–1011.
- 24 F. Hao, C. C. Stoumpos, D. H. Cao, R. P. Chang and M. G. Kanatzidis, *Nat. Photonics*, 2014, **8**, 489–494.
- 25 J. Zhang, M.-h. Shang, P. Wang, X. Huang, J. Xu, Z. Hu, Y. Zhu and L. Han, *ACS Energy Lett.*, 2016, **1**, 535–541.
- 26 R. Sheng, A. Ho-Baillie, S. Huang, S. Chen, X. Wen, X. Hao and M. A. Green, *J. Phys. Chem. C*, 2015, **119**, 3545–3549.
- 27 G. Kieslich, S. Sun and A. K. Cheetham, *Chem. Sci.*, 2015, **6**, 3430–3433.
- 28 A. L. Abdelhady, M. I. Saidaminov, B. Murali, V. Adinolfi, O. Voznyy, K. Katsiev, E. Alarousu, R. Comin, I. Dursun and L. Sinatra, *J. Phys. Chem. Lett.*, 2016, **7**, 295–301.
- 29 S. Barman and M. Sadhukhan, *J. Mater. Chem.*, 2012, **22**, 21832–21837.
- 30 G. R. Kumar, A. D. Savariraj, S. Karthick, S. Selvam, B. Balamuralitharan, H.-J. Kim, K. K. Viswanathan, M. Vijaykumar and K. Prabakar, *Phys. Chem. Chem. Phys.*, 2016, **18**, 7284–7292.
- 31 I. L. Soroka, A. Shchukarev, M. Jonsson, N. V. Tarakina and P. A. Korzhavyi, *Dalton Trans.*, 2013, **42**, 9585–9594.
- 32 G. E. Eperon, D. Bryant, J. Troughton, S. D. Stranks, M. B. Johnston, T. Watson, D. A. Worsley and H. J. Snaith, *J. Phys. Chem. Lett.*, 2014, **6**, 129–138.
- 33 M. A. Green, A. Ho-Baillie and H. J. Snaith, *Nat. Photonics*, 2014, **8**, 506–514.
- 34 T. C. Sum and N. Mathews, *Energy Environ. Sci.*, 2014, **7**, 2518–2534.